LETTER • OPEN ACCESS

Arctic summer sea ice loss will accelerate in coming decades

View the article online for updates and enhancements.

ENVIRONMENTAL RESEARCH
LETTERS

LETTER

Arctic summer sea ice loss will accelerate in coming decades

Anna Poltronieri[1,*] (ID), Nils Bochow[1,2,3] (ID), Nikolas Olson Aksamit[1] (ID), Niklas Boers[3,4,5] (ID), Per Kristen Jakobsen[1] (ID) and Martin Rypdal[1] (ID)

1 Department of Mathematics and Statistics, Faculty of Science and Technology, UiT The Arctic University of Norway, Tromsø, Norway
2 Physics of Ice, Climate and Earth, Niels Bohr Institute, University of Copenhagen, Copenhagen, Denmark
3 Potsdam Institute for Climate Impact Research, Potsdam, Germany
4 Earth System Modelling, School of Engineering & Design, Technical University of Munich, Munich, Germany
5 Department of Mathematics and Global Systems Institute, University of Exeter, Exeter, United Kingdom
* Author to whom any correspondence should be addressed.
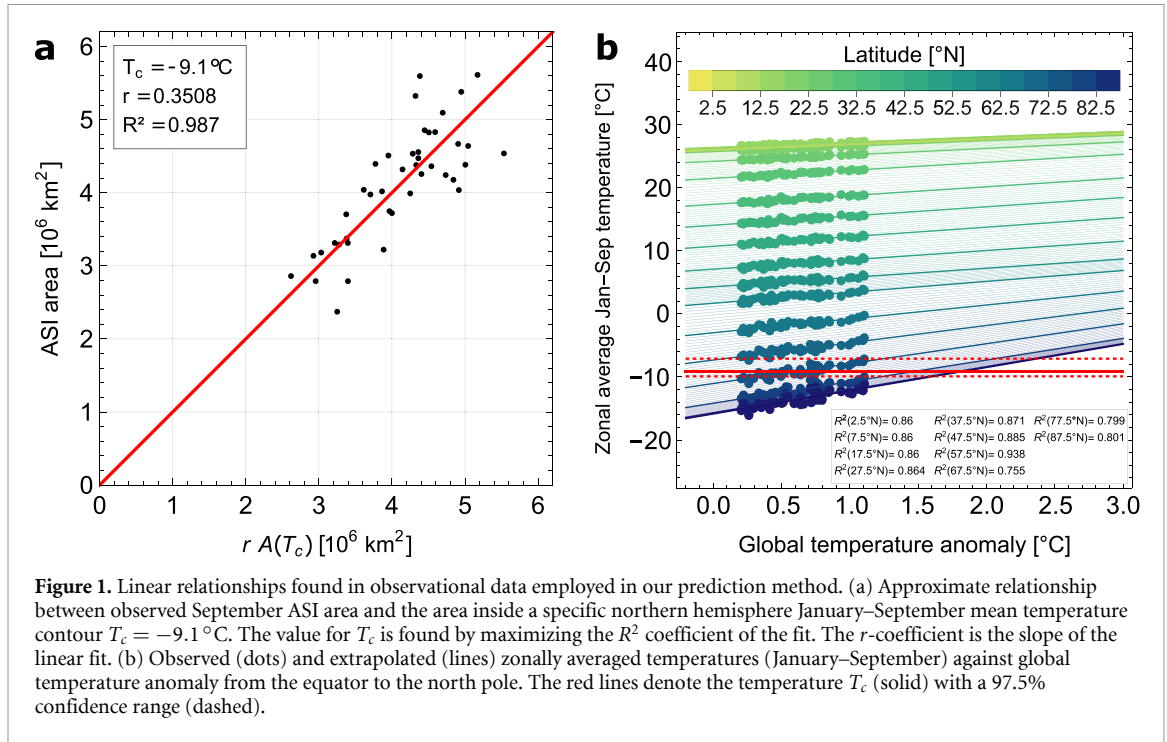
E-mail: apo050@uit.no

Abstract

The Arctic sea ice (ASI) is expected to decrease with further global warming. However, considerable uncertainty remains regarding the temperature range that would lead to a completely ice-free Arctic. Here, we combine satellite data and a large suite of models from the latest phase of the Coupled Model Intercomparison Project (CMIP6) to develop an empirical, observation-based projection of the September ASI area for increasing global mean surface temperature (GMST) values. This projection harnesses two simple linear relationships that are statistically supported by both observations and model data. First, we show that the September ASI area is linearly proportional to the area inside a specific northern hemisphere January–September mean temperature contour T_c. Second, we use observational data to show how zonally averaged temperatures have followed a positive linear trend relative to the GMST, consistent with Arctic amplification. To ensure the reliability of these observations throughout the rest of the century, we validate this trend by employing the CMIP6 ensemble. Combining these two linear relationships, we show that the September ASI area decrease will accelerate with respect to the GMST increase. Our analysis of observations and CMIP6 model data suggests a complete loss of the September ASI (area below 10^6 km^2) for global warming between 1.5 °C and 2.2 °C above pre-industrial GMST levels.

1. Introduction

The loss of Arctic sea ice (ASI) in the last decades is one of the most evident manifestations of anthropogenic climate change. ASI loss is strongly linked to Arctic amplification [1]—the enhanced heating of the Arctic relative to the global mean, as predicted by climate models [2–6] and confirmed by observations [7–9]. Several mechanisms contribute to Arctic amplification, such as the sea ice-albedo and the lapse-rate feedbacks [10]. In the colder months, further heating of the Arctic occurs due to increased emission of outgoing long-wave radiation and enhanced sensible and latent heat fluxes over newly exposed open water [11]. Additional ocean feedback mechanisms triggered by the reduction in the ASI cover have been identified, such as the seasonal memory of the ice cover and the so-called Atlantification [12, 13]. Seasonal memory

relates to the accumulation of heat in open water during summer, delaying ice formation and reducing ice thickness in winter, which can advance the timing of ice melt in subsequent seasons [13]. Atlantification is the increase of warmer and saltier Atlantic water in the Arctic Ocean [12]. Both mechanisms further reduce the ASI cover and lead to more pronounced seasonal changes.

These multiple competing feedbacks are often inadequately represented by the most recent generation of Earth System Models (ESMs) from the sixth phase of the Coupled Model Intercomparison Project (CMIP6) [14, 15]. The inter-model spread is large and the temperature range predicted by the models for a summer ice-free Arctic spans several degrees. Therefore, it is crucial to complement CMIP6 predictions of ice-free conditions with observed trends in the ASI area evolution. Reflecting this

Figure 1. Linear relationships found in observational data employed in our prediction method. (a) Approximate relationship between observed September ASI area and the area inside a specific northern hemisphere January–September mean temperature contour $T_c = -9.1\,°C$. The value for T_c is found by maximizing the R^2 coefficient of the fit. The r-coefficient is the slope of the linear fit. (b) Observed (dots) and extrapolated (lines) zonally averaged temperatures (January–September) against global temperature anomaly from the equator to the north pole. The red lines denote the temperature T_c (solid) with a 97.5% confidence range (dashed).

approach, several studies have incorporated observational data in future projections for the ASI area, reducing the uncertainty presented by the models alone [16–18].

The summer ASI area has generally followed a linear decrease with respect to the increasing global mean surface temperature (GMST) both in model simulations and observational data, despite exhibiting varying rates of decline and a slower loss observed since 2007 [19]. This linear response to the GMST is expected to persist for higher temperature anomalies [18, 20–27]. Our study combines two linear relationships supported by both observations and CMIP6 models to obtain a novel and simple observation-based methodology for predicting the September ASI evolution. Our projection correctly captures the linear dependence observed between the summer ASI and the GMST in historical data. However, we observe an accelerated, non-linear decline of the September ASI area for higher temperature anomalies. The temperature range for a September ice-free Arctic derived from our prediction method spans from $1.5\,°C$ to $2.2\,°C$ GMST levels above pre-industrial. This result notably reduces the uncertainty compared to the CMIP6 model projections and suggests a lower temperature threshold for the onset of ice-free summers in the Arctic, generally assumed to be at least $2\,°C$ above pre-industrial levels [16–18].

2. Methods

2.1. Observational data

We employ a satellite-based time series [28] for the September ASI area from 1979 to 2020, denoted A_{ASI}, and the zonally averaged January–September

surface temperature time series obtained from the HadCRUT5 data set [29]. For each year between 1979 and 2020, the average temperature is obtained for each $5°$-zone in the northern hemisphere. Since our prediction method relies on temperature data to estimate the yearly September ASI cover, we have chosen to utilize the average temperatures from January to September. We exclude months that do not contribute to ASI area changes for the given year, i.e. months following September.

First, we observe a linear dependence between the September ASI area and the area inside a northern hemisphere January–September mean temperature contour T_c (figure 1(a)). Second, we observe a linear dependence of the zonal average January–September temperature for each latitude θ and the GMST anomaly T_a with respect to pre-industrial levels (figure 1(b)) that can be described by the equation

$$T(\theta) = a(\theta)\,T_a + b(\theta) \tag{1}$$

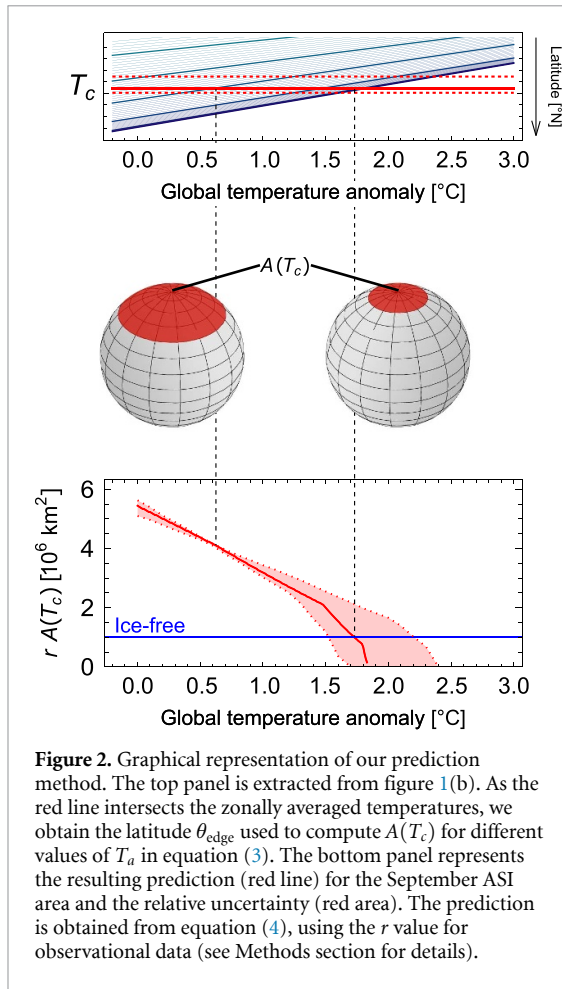The solution to the equation

$$T(\theta) = T_c \tag{2}$$

which represents the temperature contour T_c (red line in figure 1(b)) crossing the zonally averaged temperatures for different values of T_a, gives the value of $\theta = \theta_{edge}$ used in the equation

$$A(T_c) = 2\pi R^2 \int_{\theta_{edge}}^{\pi/2} \cos(\theta)\,\mathrm{d}\theta, \tag{3}$$

with the radius of the Earth $R = 6371$ km.

Figure 2. Graphical representation of our prediction method. The top panel is extracted from figure 1(b). As the red line intersects the zonally averaged temperatures, we obtain the latitude θ_{edge} used to compute $A(T_c)$ for different values of T_a in equation (3). The bottom panel represents the resulting prediction (red line) for the September ASI area and the relative uncertainty (red area). The prediction is obtained from equation (4), using the r value for observational data (see Methods section for details).

Figure 3. Observation-based projection of the September ASI area compared to CMIP6 models and linear extrapolation of observational data (1979–2020). The thin gray curves are the September ASI areas for the different CMIP6 models under the Historical + SSP5-8.5 scenario. The filled grey area corresponds to one standard deviation of the average temperature anomaly of complete ASI loss obtained from the CMIP6 models ($2.25 \pm 0.52\,°C$ above pre-industrial). The red curve and area depict the observation-based projection of the September ASI area and the relative uncertainty, respectively (see Methods section for details). The black solid curve is the observational September ASI data and the dashed line represents its linear extrapolation for higher GMST. Our observation-based projection predicts ice-free conditions for lower GMST values compared to both the CMIP6 ensemble and the linear extrapolation of observational data.

The area $A(T_c)$, when multiplied by a factor r, gives the best approximation of the observed A_{ASI} for a given value of T_a
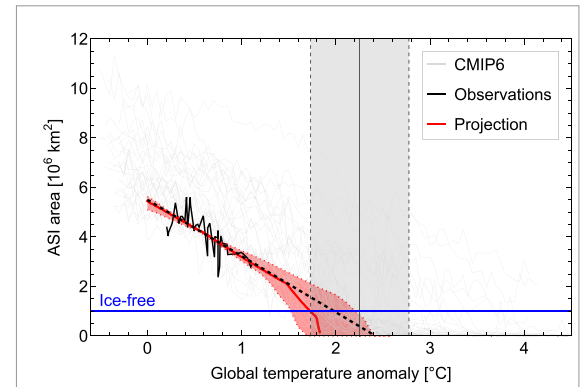
$$A_{ASI} = rA(T_c). \qquad (4)$$

The factor r is estimated via linear regression for a range of different values of T_c. The best fit for observational data, measured using the coefficient of determination R^2, is obtained for $T_c = -9.1\,°C$ (figure 1(a)). Finally, the relationship in equation (4) allows us to get the observation-based projection for the chosen T_a. A visual representation of our prediction method is depicted in figure 2.

The uncertainty in the prediction (figure 3, red area) is obtained by a Monte Carlo method. In each realization of the Monte Carlo sampling, we subtract the linear trend from the September ASI area, randomize the fluctuations, and add the randomized data to the linear trend. On the resulting data, we carry out the analysis as described above.

2.2. CMIP6 data

Our prediction method relies on the validity of the linear relationships depicted in figure 1 and on the assumption that they will hold for higher GMST anomalies than present-day conditions. To ensure the

validity of these relationships in the future, we employ different model runs from the CMIP6 ensemble. The contributions of observational data and CMIP6 models in our analysis are concisely described in figure 4.
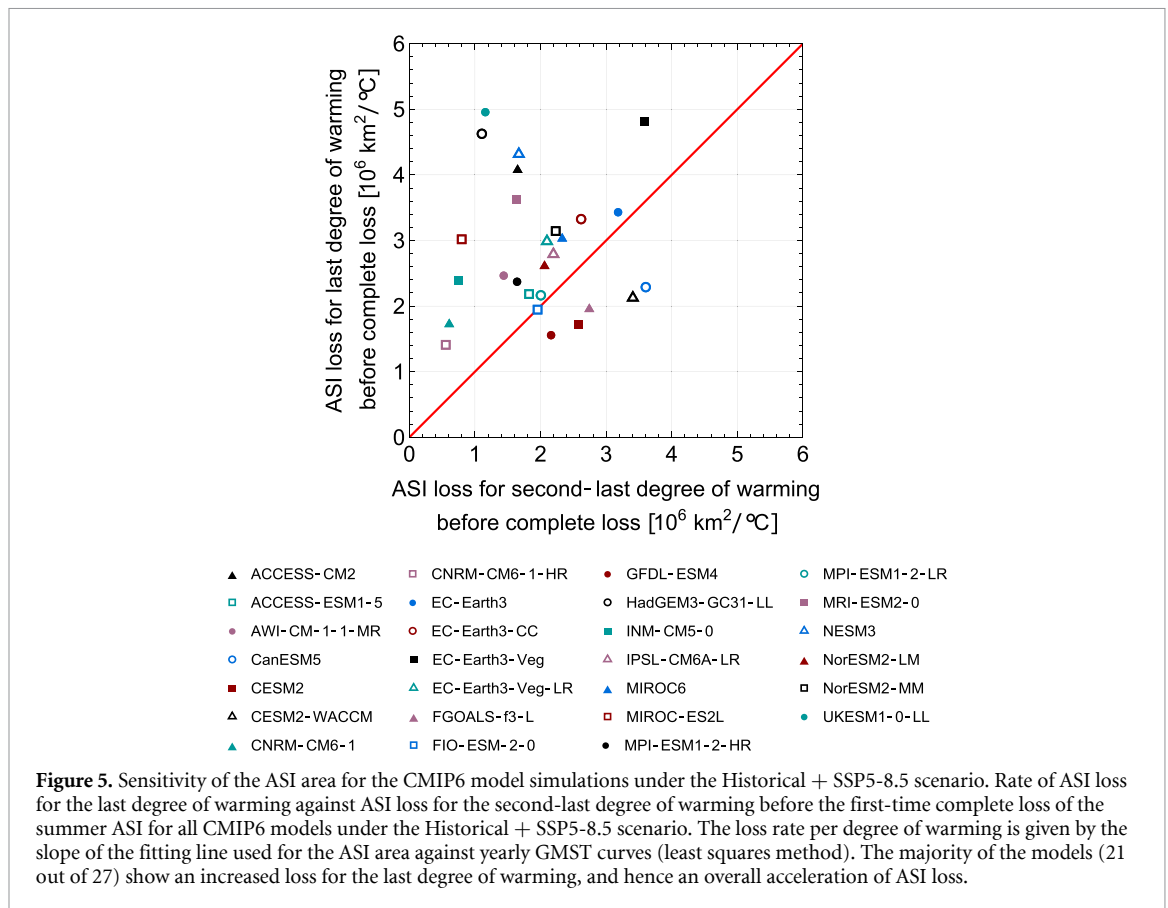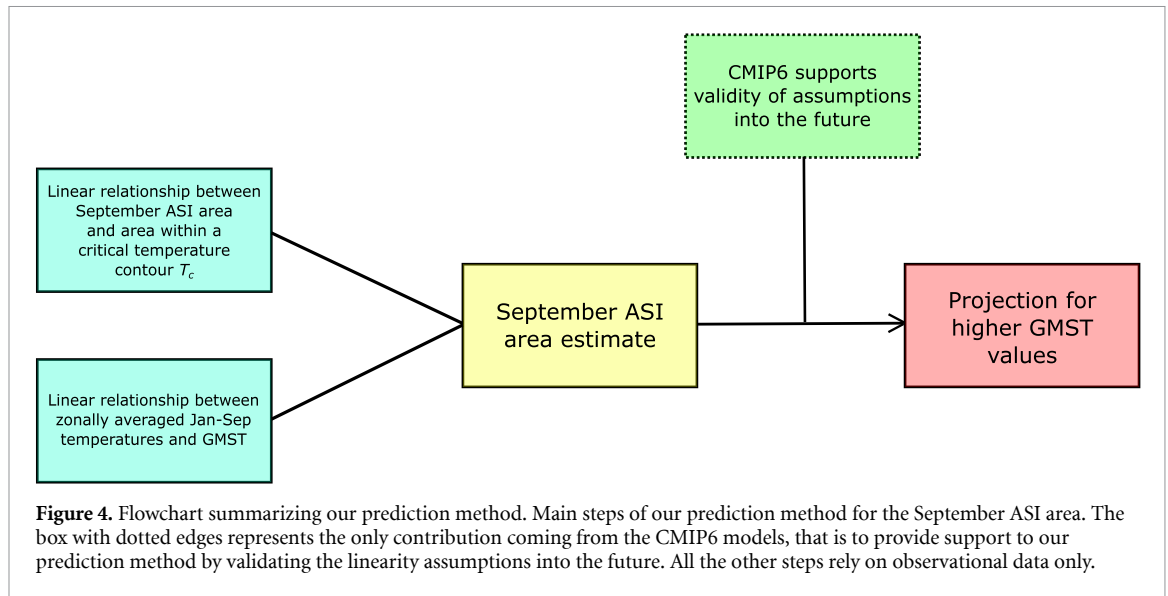
We merge data from the Historical and the SSP5-8.5 (Shared Socioeconomic Pathway scenario with very high levels of greenhouse gas emissions) simulations for 30 CMIP6 models, up to the year 2100. We use the monthly averaged variables `siarean` (sea ice area north) and `siconc` (sea ice concentration). For the temperature, we use `tas` (temperature at the surface). As for the observational data, we fit linear functions to the data with zero intercept and find the value for the temperature T_c for every model by maximizing R^2 (figure S5).

2.3. ASI sensitivity

We estimate the sensitivity of the ASI area as the rate of ASI loss per degree of warming before the complete loss of the summer ASI in three different CMIP6 scenarios: Historical + SSP5-8.5, Historical + SSP2-4.5 (Shared Socioeconomic Pathway with intermediate levels of greenhouse gas emissions), and 1pctCO2 (gradual 1% increase in CO_2 concentration per year).

We fit the ASI area against temperature anomaly curves using a least squares method with the slope representing the average loss rate of ice per degree of warming (figures 5, S1(a) and S2(a)). We repeat the analysis by fitting the curves using a total least squares method (figures S1(b), S2(b) and S3). We find that most models exhibit a higher rate of September ASI

Figure 4. Flowchart summarizing our prediction method. Main steps of our prediction method for the September ASI area. The box with dotted edges represents the only contribution coming from the CMIP6 models, that is to provide support to our prediction method by validating the linearity assumptions into the future. All the other steps rely on observational data only.

Figure 5. Sensitivity of the ASI area for the CMIP6 model simulations under the Historical + SSP5-8.5 scenario. Rate of ASI loss for the last degree of warming against ASI loss for the second-last degree of warming before the first-time complete loss of the summer ASI for all CMIP6 models under the Historical + SSP5-8.5 scenario. The loss rate per degree of warming is given by the slope of the fitting line used for the ASI area against yearly GMST curves (least squares method). The majority of the models (21 out of 27) show an increased loss for the last degree of warming, and hence an overall acceleration of ASI loss.
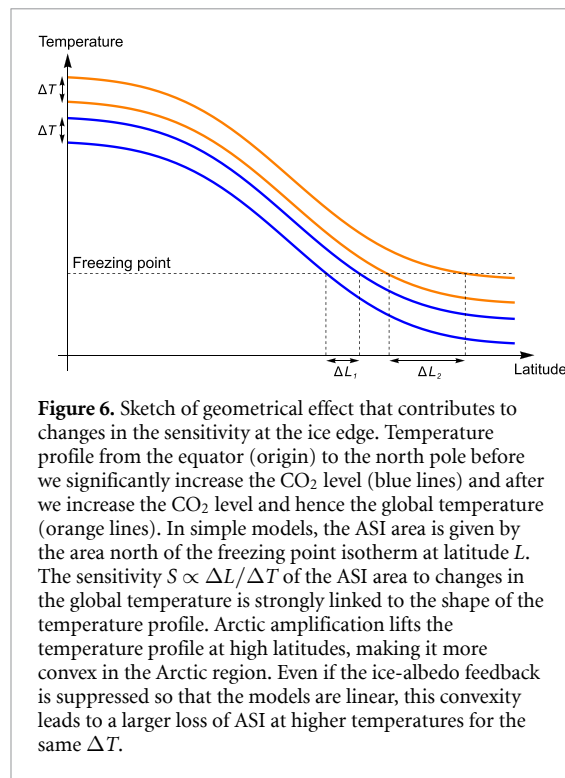
decline for the last degree of warming before the complete ASI loss, compared to the second-last degree. While the exact rate of ASI area loss is sensitive to the choice of linear fitting methodology, most models show an accelerated loss of the ASI under both fittings, with slight variation across scenarios.

2.4. Temperature anomaly of complete ASI loss
To calculate the yearly GMST anomalies, we subtract the globally averaged temperature from 1850 to 1900

AD of the data set in use from the same temperature time series. This provides anomaly values relative to the pre-industrial period. In the CMIP6 models under consideration, the pre-industrial average temperatures range from $12.4\,°C$ to $15.3\,°C$, with mean $13.6\,°C$ and one standard deviation $0.65\,°C$. The pre-industrial average temperature in the HadCRUT5 data set is $13.8\,°C$. In some model runs the ASI area fluctuates around the threshold for an ice-free Arctic of 10^6 km^2 after the ASI is completely lost for the

Figure 6. Sketch of geometrical effect that contributes to changes in the sensitivity at the ice edge. Temperature profile from the equator (origin) to the north pole before we significantly increase the CO_2 level (blue lines) and after we increase the CO_2 level and hence the global temperature (orange lines). In simple models, the ASI area is given by the area north of the freezing point isotherm at latitude L. The sensitivity $S \propto \Delta L/\Delta T$ of the ASI area to changes in the global temperature is strongly linked to the shape of the temperature profile. Arctic amplification lifts the temperature profile at high latitudes, making it more convex in the Arctic region. Even if the ice-albedo feedback is suppressed so that the models are linear, this convexity leads to a larger loss of ASI at higher temperatures for the same ΔT.

first time. Therefore, we smooth the ASI area against temperature anomaly curves using a $1\,°C$ centered moving average and determine the temperature of the complete ASI loss from the smoothed data. We average these values and find that the mean temperature anomaly for the complete September ASI loss for the models is $2.25\,°C$ with one standard deviation $0.52\,°C$ above pre-industrial GMST levels under the Historical + SSP5-8.5 scenario (filled gray area in figure 3) and $2.03 \pm 0.34\,°C$ under Historical + SSP2-4.5. Note that the smoothed curves are only used to determine the temperature of the complete ASI loss, not for the previous sensitivity analysis.

2.5. Analysis on a different observational data set

We confirm the robustness of our results by repeating the analysis on an independent observational sea ice data set, the Sea Ice Index, Version 3 [30]. This additional observation-based projection confirms our conclusions and exhibits an accelerated non-linear decline of the ASI area with ice-free conditions predicted for global warming between $1.5\,°C$ and $2.2\,°C$ above pre-industrial GMST levels (figure S4).

3. Results

The linear proportionality between the September ASI area and the area inside the mean temperature contour holds for different values of T_c, depending on the dataset under consideration. For the observational data, the best approximation (measured using R^2) of the temperature contour is $T_c = -9.1\,°C$ (figure 1(a)). The same linear dependence holds for

all the CMIP6 models considered under the Historical + SSP5-8.5 scenario with $R^2 > 0.95$ (figure S5(b)), though the temperature T_c that gives the best approximation slightly varies. Across CMIP6, T_c ranges from $-14.3\,°C$ to $-6.8\,°C$, with mean $-10.8\,°C$ and one standard deviation $1.7\,°C$ (figure S5(a)). While the spread in the T_c values across the models may be attributed to differences in their internal climate dynamics or parameterization schemes, the consistent linear dependency of the September ASI area on the area delimited by the temperature contour T_c that exists in all CMIP6 models supports our methodology. There is also a linear dependence between the September ASI area and the January-September mean Arctic temperature (above 66°N), but the R^2 values show that this dependence is not as concise as the one shown in our approach, both in observational data and in CMIP6 models (table S1 and figure S6).

The linear proportionality between the September ASI area and the area inside the temperature contour T_c, combined with the linear trend of the zonal temperature for higher GMST anomalies, constitutes our prediction method (figure 3). The result is a purely observation-based projection of the September ASI area that shows an accelerating, non-linear decline for increasing GMST anomalies, with a smaller uncertainty range than CMIP6 projections. From these observations, we can predict ice-free conditions (area below 10^6 km^2) for global warming between $1.5\,°C$ and $2.2\,°C$ above pre-industrial GMST levels. The predicted decline in the September ASI area is based purely on the satellite-based observational record and the identified strong relationships with the temperatures.

Most of the CMIP6 models that reach ice-free conditions under the Historical + SSP5-8.5 scenario are aligned with the accelerating, non-linear decline that we observe in our projection. These models show an increased loss of ASI for the last degree of warming, compared to the second-last degree, before reaching ice-free conditions in September (models above the red line in figures 5 and S3). We repeat the sensitivity analysis on the models that reach ice-free conditions under the Historical + SSP2-4.5 and 1pctCO2 scenarios (figures S1–S2). We observe again that the majority of the models show an accelerated loss of ASI for the last degree of warming, compared to the second-last degree, before reaching ice-free conditions in September.

4. Discussion

In this study, we combine two linear relationships, both backed by observational data and CMIP6 models, to develop a new and simple methodology based on observations for forecasting the evolution of the September ASI area.

Our methodology is inspired by energy-balance models (EBMs), where the ASI area is defined as the region north of a zonally-averaged temperature isotherm. This definition shows that the ASI decline can vary in pace, accelerating or decelerating, independent of Arctic amplification, based on the temperature gradient at the ice edge (figure 6). Inspired by the existence of this non-linearity in such simple models, we test for the presence of similar behavior in both CMIP6 model data and observations.

First, we find a similar EBM-type linear proportionality between the September ASI area and the area inside a northern hemisphere January-September mean temperature contour T_c (figures 1(a) and S5). Second, we find a linear dependence of the zonally averaged January-September temperatures and the GMST anomaly (figures 1(b) and S7–S14), which is predicted to persist through the end of the century by the CMIP6 models. Combining these linear relationships allows us to obtain an observation-based projection for the September ASI area. Our projection correctly reproduces the observed historical linear decline of the September ASI area in response to the increasing GMST [18, 20–27]. However, we detect an accelerated, non-linear decline of the summer ASI area for higher GMST values (figure 3).

The CMIP6 models suggest that the sensitivity of the ASI area will increase with higher temperatures, as informed by the observation-based projection. The majority of the models analyzed show a higher rate of ASI loss for the last degree of warming, compared to the second-last degree, before reaching ice-free summers under different scenarios (figures 5 and S1–S3). Despite the general problems of state-of-the-art coupled climate models to estimate the sensitivity of the ASI area to warming [31, 32], this result suggests a potential acceleration towards an ice-free Arctic.

Numerous studies have already narrowed the large uncertainty presented by the ESMs when estimating the temperature increase required for the onset of ice-free summers in the Arctic [16–18]. A novel Bayesian approach [16] and model simulations recalibrated using observations [17, 18] suggest that the Arctic is likely to become ice-free in summer for global warming of at least $2\,^{\circ}\text{C}$ above pre-industrial levels. Our method projects an earlier temperature range for the occurrence of complete sea ice loss in summer, estimating the GMST anomalies required for a September ice-free Arctic to be between $1.5\,^{\circ}\text{C}$ and $2.2\,^{\circ}\text{C}$ above pre-industrial levels.

Using the averaged GMST data from the analyzed CMIP6 models, we convert the obtained temperature range to dates for a summer ice-free Arctic. This gives us the onset of a September ice-free Arctic between 2027 and 2045 under the SSP5-8.5 scenario (very high emissions) and between 2030 and 2059 under the SSP2-4.5 scenario (intermediate emissions).

It is important to note that the validity of our prediction depends on the CMIP6 models' suggestion that a linear dependence of the zonally averaged temperatures on the GMST anomaly will persist throughout the century. As we rely on this linearity assumption to extend our observation-based projection into the future, a different type of behavior would affect the predicted trajectory for the ASI, either decelerating or further accelerating its loss. However, our method does not rely on the CMIP6 models' ability to reproduce or predict the ASI cover evolution.

Data availability statement

Acknowledgment

Author contributions

A P, N Boc, P K J, and M R conceived the study. A P performed the analysis. All authors discussed and interpreted the results. A P wrote the paper with contributions from the other authors.

Conflict of interests

The authors declare that they have no competing financial interests.

ORCID iDs

Anna Poltronieri ● https://orcid.org/0000-0001-7101-3456
Nils Bochow ● https://orcid.org/0000-0003-4578-5780
Nikolas Olson Aksamit ● https://orcid.org/0000-0002-2610-7258
Niklas Boers ● https://orcid.org/0000-0002-1239-9034
Per Kristen Jakobsen ● https://orcid.org/0000-0003-4197-5309
Martin Rypdal ● https://orcid.org/0000-0003-0053-665X

References

[1] Kumar A, Perlwitz J, Eischeid J, Quan X, Xu T, Zhang T, Hoerling M, Jha B and Wang W 2010 Contribution of sea ice loss to Arctic amplification *Geophys. Res. Lett.* **37** L21701

[2] Holland M M and Bitz C M 2003 Polar amplification of climate change in coupled models *Clim. Dyn.* **21** 221–32

[3] Stroeve J C, Kattsov V, Barrett A, Serreze M, Pavlova T, Holland M and Meier W N 2012 Trends in Arctic sea ice extent from CMIP5, CMIP3 and observations *Geophys. Res. Lett.* **39** L16502

[4] Smith D M *et al* 2019 The Polar Amplification Model Intercomparison Project (PAMIP) contribution to CMIP6: investigating the causes and consequences of polar amplification *Geosci. Model Dev.* **12** 1139–64

[5] Barnes E A and Polvani L M 2015 CMIP5 projections of Arctic amplification, of the North American/North Atlantic circulation and of their relationship *J. Clim.* **28** 5254–527

[6] Davy R and Outten S 2020 The Arctic surface climate in CMIP6: status and developments since CMIP5 *J. Clim.* **33** 8047–806

[7] Serreze M C and Francis J A 2006 The Arctic amplification debate *Clim. Change* **76** 241–64

[8] Serreze M C, Barrett A P, Stroeve J C, Kindig D N and Holland M M 2009 The emergence of surface-based Arctic amplification *Cryosphere* **3** 11–19

[9] Screen J A and Simmonds I 2010 The central role of diminishing sea ice in recent Arctic temperature amplification *Nature* **464** 1334–7

[10] Graversen R G and Wang M 2009 Polar amplification in a coupled climate model with locked albedo *Clim. Dyn.* **33** 629–43

[11] Dai A, Luo D, Song M and Liu J 2019 Arctic amplification is caused by sea-ice loss under increasing CO_2 *Nat. Commun.* **10** 121

[12] Polyakov I V *et al* 2017 Greater role for Atlantic inflows on sea-ice loss in the Eurasian basin of the Arctic ocean *Science* **356** 285–91

[13] Ivanov V 2023 Arctic sea ice loss enhances the oceanic contribution to climate change *Atmosphere* **14** 409

[14] Eyring V, Bony S, Meehl G A, Senior C A, Stevens B, Stouffer R J and Taylor K E 2016 Overview of the coupled model intercomparison project phase 6 (CMIP6) experimental design and organization *Geosci. Model Dev.* **9** 1937–58

[15] Keen A *et al* 2021 An inter-comparison of the mass budget of the Arctic sea ice in CMIP6 models *Cryosphere* **15** 951–82

[16] Olson R, An S I, Fan Y, Chang W, Evans J P and Lee J Y 2019 A novel method to test non-exclusive hypotheses applied to Arctic ice projections from dependent models *Nat. Commun.* **10** 3016

[17] Niederdrenk A L and Notz D 2018 Arctic sea ice in a 1.5°C warmer world *Geophys. Res. Lett.* **45** 1963–71

[18] Mahlstein I and Knutti R 2012 September Arctic sea ice predicted to disappear near 2°C global warming above present *J. Geophys. Res. Atmos.* **117** D06104

[19] Perovich D *et al* 2020 Arctic report card 2020: sea ice (available at: https://repository.library.noaa.gov/view/noaa/27904)

[20] Gregory J M, Stott P A, Cresswell D J, Rayner N A, Gordon C and Sexton D M H 2002 Recent and future changes in Arctic sea ice simulated by the HadCM3 AOGCM *Geophys. Res. Lett.* **29** 28–1–28–4

[21] Winton M 2011 Do climate models underestimate the sensitivity of Northern hemisphere sea ice cover? *J. Clim.* **24** 3924–34

[22] Ridley J K, Lowe J A and Hewitt H T 2012 How reversible is sea ice loss? *Cryosphere* **6** 193–8

[23] Li C, Notz D, Tietsche S and Marotzke J 2013 The transient versus the equilibrium response of sea ice to global warming *J. Clim.* **26** 5624–36

[24] Stroeve J and Notz D 2015 Insights on past and future sea-ice evolution from combining observations and models *Glob. Planet. Change* **135** 119–32

[25] Rosenblum E and Eisenman I 2016 Faster Arctic sea ice retreat in CMIP5 than in CMIP3 due to volcanoes *J. Clim.* **29** 9179–88

[26] Jahn A 2018 Reduced probability of ice-free summers for 1.5°C compared to 2°C warming *Nat. Clim. Change* **8** 409–13

[27] Notz D and Stroeve J 2018 The trajectory towards a seasonally ice-free Arctic ocean *Curr. Clim. Change Rep.* **4** 407–16

[28] Stroeve J and Meier W N 2018 Sea ice trends and climatologies from SMMR and SSM/I-SSMIS, version 3, gsfc.nasateam.month.area.1978-2020.n *NASA National Snow and Ice Data Center Distributed Active Archive Center*

[29] Morice C P, Kennedy J J, Rayner N A, Winn J P, Hogan E, Killick R E, Dunn R J H, Osborn T J, Jones P D and Simpson I R 2021 An updated assessment of near-surface temperature change from 1850: the HadCRUT5 data set *J. Geophys. Res. Atmos.* **126** e2019JD032361

[30] Fetterer F, Knowles K, Meier W N, Savoie M and Windnagel A K 2017 *Sea Ice Index, Version 3. N_09_extent_v3.0.csv* (NSIDC: National Snow and Ice Data Center)

[31] Horvat C 2021 Marginal ice zone fraction benchmarks sea ice and climate model skill *Nat. Commun.* **12** 2221

[32] Notz D and Community SIMIP 2020 Arctic sea ice in CMIP6 *Geophys. Res. Lett.* **47** e2019GL086749